Inorganic Chemistry

Article

A Family of [Mn₆] Complexes Featuring Tripodal Ligands

Constantinos J. Milios,[†] Maria Manoli,[†] Gopalan Rajaraman,[‡] Abhudaya Mishra,[§] Laura E. Budd,[†] Fraser White,[†] Simon Parsons,[†] Wolfgang Wernsdorfer,[||] George Christou,[§] and Euan K. Brechin*,[†,‡]

School of Chemistry, The University of Edinburgh, West Mains Road, Edinburgh EH9 3JJ, U.K., Department of Chemistry, The University of Manchester, Oxford Road, Manchester M13 9PL, U.K., Department of Chemistry, University of Florida, Gainesville, Florida 32611-7200, and Laboratoire Louis Néel, CNRS, 38042 Grenoble Cedex 9, France

The synthesis and magnetic properties of four new Mn complexes containing tripodal alcohol ligands are reported: [Mn₆(OAc)₆(H₂tea)₂(tmp)₂]·2MeCN (**1**·2MeCN), [Mn₆(acac)₄(OAc)₂(Htmp)₂(H₂N-ep)₂] (**2**), [Mn₆(OAc)₈(tmp)₂(py)₄]·2py (**3**·2py), and [Mn₆(OAc)₈(thme)₂(py)₄]·2py (**4**·2py) [H₃tea, triethanolamine; H₃tmp, 1,1,1-tris(hydroxymethyl)propane; H₂N–H₂ep, 2-amino-2-ethyl-1,3-propanediol; H₃thme, 1,1,1-tris(hydroxymethyl)ethane]. All complexes are mixed-valent with a [Mn^{III}₂Mn^{II}₄] oxidation assignment and are constructed from four edge-sharing triangles but differ slightly in that complexes **1** and **2** display a [Mn^{III}₂Mn^{II}₄(μ_2-OR)₆(μ_3-OR)₄]$^{4+}$ core, while complexes **3** and **4** feature [Mn^{III}₂Mn^{II}₄(μ_2-OR)₂(μ_3-OR)₄]$^{8+}$ and [Mn^{III}₂Mn^{II}₄(μ_2-OR)₄(μ_3-OR)₄]$^{6+}$ cores, respectively. dc and ac magnetic susceptibility studies in the 2–300 K range for complexes **1**–**4** reveal the presence of dominant antiferromagnetic exchange interactions, leading to ground states of $S = 0$ for **1** and **2**, while complexes **3** and **4** display $S = 4$ ground states with $D = -0.44$ and -0.58 cm^{-1}, respectively. Single-molecule magnetism behavior was confirmed for **3** and **4** by the presence of sweep-rate and temperature-dependent hysteresis loops in single-crystal *M* vs *H* studies at temperatures down to 40 mK. Theoretical density functional calculations were used to evaluate the individual pairwise exchange interactions present, confirming the diamagnetic ground states for **1** and **2** and the $S = 4$ ground states for **3** and **4**.

Introduction

One of the most intriguing recent developments in molecular magnetism is the discovery that simple coordination compounds containing paramagnetic metal ions can function as single-domain magnetic particles at low temperatures in the absence of an external magnetic field. Such molecules, now termed "single-molecule magnets" (SMMs), exist if two criteria are met, namely, a large (or at least nonzero) spin ground state (*S*) and a large magnetoanisotropy of the Ising (easy-axis) type (as measured by the (negative) zero-field-splitting parameter, *D*).[1] As such, these molecules represent the ultimate down-limit in the scale of magnetic materials and potentially promise unique applications in information

storage and quantum computation.[2] Since the discovery of the phenomenon,[3] many complexes have been found to possess such behavior, and while the vast majority of these contain Mn ions in various oxidation states,[4] there have been reported examples of Fe, V, Co, Ni, and, very recently, combinations of 3d with 4d, 5d, and 4f paramagnetic ions.[5−9]

An important future development for the SMM field is the discovery of synthetic schemes that can yield new molecules and families of related molecules with large spins and/or significant magnetoanisotropies. Toward this end, two successful methodologies have emerged: the first is based on "serendipitous self-assembly", whereby suitable flexible

---

* To whom correspondence should be addressed. E-mail: ebrechin@staffmail.ed.ac.uk.
† The University of Edinburgh.
‡ The University of Manchester.
§ University of Florida.
|| Laboratoire Louis Néel, CNRS.

(1) (a) Gatteschi, D.; Sessoli, R. *Angew. Chem., Int. Ed.* **2003**, *42*, 268. (b) Christou, G.; Gatteschi, D.; Hendrickson, D. N.; Sessoli, R. *MRS Bull.* **2000**, *25*, 66.

(2) Representative references include: (a) Tejada, J.; Chudnovsky, E. M.; del Barco, E.; Hernandez, J. M.; Spiller, T. P. *Nanotechnology* **2001**, *12*, 181. (b) Stamp, P. C. *Nature* **1996**, *383*, 125. (c) Wernsdorfer, W.; Sessoli, R. *Science* **1999**, *284*, 133.

(3) (a) Lis, T. *Acta Crystallogr.* **1980**, *B36*, 2042. (b) Caneschi, A.; Gatteschi, D.; Sessoli, R.; Barra, A. L.; Brunel, L. C.; Guillot, M. *J. Am. Chem. Soc.* **1991**, *113*, 5873. (c) Sessoli, R.; Tsai, H. L.; Schake, A. R.; Wang, S. Y.; Vincent, J. B.; Folting, K.; Gatteschi, D.; Christou, G.; Hendrickson, D. N. *J. Am. Chem. Soc.* **1993**, *115*, 1804. (d) Sessoli, R.; Gatteschi, D.; Caneschi, A.; Novak, M. A. *Nature* **1993**, *365*, 141.

bridging ligands (e.g., carboxylates) are mixed with simple metal salts or premade polymetallic compounds in a particular solvent or mixture of solvents,[9] and the second is the "rational design" of molecules, whereby inflexible ligands (e.g., cyanide) direct the formation of complexes whose overall formulas and topology can, in many cases, be wholly or partly predicted, suggesting a more "customized" preparation of SMMs.[10] The understanding and interpretation of the factors that determine why individual complexes display large spin ground states and SMM behavior is clearly important, and this requires the formation and study of families of related SMMs so that structure−property relations can be developed.

From our previous experience of employing tripodal alcohol ligands in manganese carboxylate chemistry, we have been able to isolate high-spin molecules and SMMs with nuclearities ranging from 2 to 32, suggesting that such ligands are indeed excellent candidates for the preparation of

Chart 1. Structures of H_3thme, H_3tmp, H_3tea, and H_2N-H_2ep
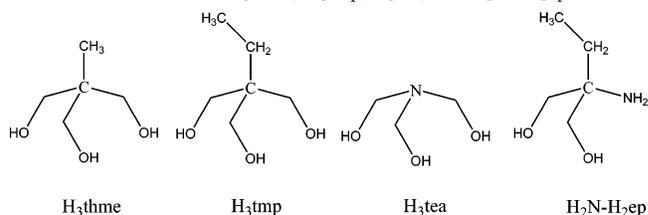
polynuclear Mn complexes with interesting magnetic properties.[8d,11] The majority of these complexes have been isolated using the basic manganese carboxylate "triangles" of general formula $[Mn_3O(O_2CR)_6L_3]^{0/+}$ (R = Me, Ph, etc.; L = py, MeCN, H_2O, etc.), and we therefore decided to extend these studies to include the use of manganese β-diketonate salts and various other "simple" Mn sources. Herein we report the syntheses, structures, and magnetic properties of a new family of hexanuclear Mn clusters built with tripodal ligands (Chart 1). All four complexes display very similar structures, yet their observed magnetic behavior ranges from $S = 0$ ground states to single-molecule magnetism, and this allows us to examine the effect that subtle changes in geometry have on the nature of the individual pairwise exchange interactions and the resultant ground states.

Experimental Section

All manipulations were performed under aerobic conditions, using materials as received. $[Mn_3O(OAc)_6(py)_3]\cdot py$, $NBu_4^nMnO_4$, and $[Mn_{12}O_{12}(OAc)_{16}(H_2O)_4]\cdot 2CH_3COOH\cdot 4H_2O$ were prepared as previously described.[3c,12]

$[Mn_6(OAc)_6(H_2tea)_2(tmp)_2]\cdot 2MeCN$ (1·2MeCN). To a stirred suspension of $Mn(acac)_2$ (0.500 g, 1.97 mmol) in CH_3CN (30 mL) were added 1,1,1-tris(hydroxymethyl)propane (H_3tmp; 0.265 g, 1.97 mmol) and triethanolamine (H_3tea; 0.331 g, 1.97 mmol). The resulting yellow-brown suspension was left stirring overnight, during which time it changed to dark brown. The solution was filtered through Celite and layered with two volumes of *n*-hex/ Et_2O (1/1). After 1 week, the dark-brown crystals formed were isolated by filtration, washed with Et_2O, and dried in vacuo; yield ∼35%. A sample for X-ray crystallography was kept in the mother liquor to prevent solvent loss. Anal. Calcd (found) for $[Mn_6(OAc)_6(H_2$tea)$_2$(tmp)$_2]\cdot 2MeCN$ (1·2MeCN): C, 36.38 (36.62); H, 5.34 (5.35); N, 4.24 (4.09). Selected IR data (KBr disk, cm^{-1}): 1564vs, 1417vs, 1340m, 1280m, 1246w, 1228m, 1116s, 1054s, 944m, 903s, 857w, 773m, 657s, 602m, 556s, 502m.

(4) (a) Hendrickson, D. N.; Christou, G.; Ishimoto, H.; Yoo, J.; Brechin, E. K.; Yamaguchi, A.; Rumberger, E. M.; Aubin, S. M. J.; Sun, Z.; Aromi, G. *Polyhedron* **2001**, *20*, 1479. (b) Boskovic, C.; Brechin, E. K.; Streib, W. E.; Folting, K.; Bollinger, J. C.; Hendrickson, D. N.; Christou, G. *J. Am. Chem. Soc.* **2002**, *124*, 3725. (c) Soler, M.; Rumberger, E. M.; Folting, K.; Hendrickson, D. N.; Christou, G. *Polyhedron* **2001**, *20*, 1365. (d) Cadiou, C.; Murrie, M.; Paulsen, C.; Villar, V.; Wernsdorfer, W.; Winpenny, R. E. P. *Chem. Commun.* **2001**, 2666. (e) Brechin, E. K.; Soler, M.; Davidson, J.; Hendrickson, D. N.; Parsons, S.; Christou, G. *Chem. Commun.* **2002**, 2252. (f) Jones, L. F.; Brechin, E. K.; Collison, D.; Harrison, A.; Teat, S. J.; Wernsdorfer, W. *Chem. Commun.* **2002**, 2974. (g) Milios, C. J.; Raptopoulou, C. P.; Terzis, A.; Lloret, F.; Vicente, R.; Perlepes, S. P.; Escuer, A. *Angew. Chem., Int. Ed.* **2004**, *43*, 210. (h) Price, J. P.; Batten, S. R.; Moubaraki, B.; Murray, K. S. *Chem. Commun.* **2002**, 762. (i) Goodwin, J. C.; Sessoli, R.; Gatteschi, D.; Wernsdorfer, W.; Powell, A. K.; Heath, S. L. *J. Chem. Soc., Dalton Trans.* **2000**, 1835. (j) Andres, H.; Basler, R.; Blake, A. J.; Cadiou, C.; Chaboussant, G.; Grant, C. M.; Güdel, H.-U.; Murrie, M.; Parsons, S.; Paulsen, C.; Semadini, F.; Villar, V.; Wernsdorfer, W.; Winpenny, R. E. P. *Chem.− Eur. J.* **2002**, *8*, 4867. (k) Berlinguette, C. P.; Vaughn, D.; Cañada-Vilalta, C.; Galan-Mascaras, J. R.; Dunbar, K. R. *Angew. Chem., Int. Ed.* **2003**, *42*, 1523. (l) Sokol, J. J.; Hee, A. G.; Long, J. R. *J. Am. Chem. Soc.* **2002**, *124*, 7656. (m) Sañudo, E. C.; Wernsdorfer, W.; Abboud, K. A.; Christou, G. *Inorg. Chem.* **2004**, *43*, 4137. (n) Soler, M.; Wernsdorfer, W.; Folting, K.; Pink, M.; Christou, G. *J. Am. Chem. Soc.* **2004**, *126*, 2156. (o) Tasiopoulos, A.; Vinslava, A.; Wernsdorfer, W.; Abboud, K. A.; Christou, G. *Angew. Chem., Int. Ed.* **2004**, *43*, 2117. (p) Brechin, E. K.; Sañudo, E. C.; Wernsdorfer, W.; Boskovic, C.; Yoo, J.; Hendrickson, D. N.; Yamaguchi, A.; Ishimoto, H.; Concolino, T. E.; Rheingold, A. L.; Christou, G. *Inorg. Chem.* **2005**, *44*, 502.

(5) (a) Blake, A. J.; Grant, C. M.; Parsons, S.; Rawson, J. M.; Winpenny, R. E. P. *J. Chem. Soc., Chem. Commun.* **1994**, 2363. (b) Cadiou, C.; Murrie, M.; Paulsen, C.; Villar, V.; Wernsdorfer, W.; Winpenny, R. E. P. *Chem. Commun.* **2001**, 2666. (c) Moragues-Cánovas, M.; Helliwell, M.; Ricard, L.; Rivière, E.; Wernsdorfer, W.; Brechin, E. K.; Mallah, T. *Eur. J. Inorg. Chem.* **2004**, 2219. (d) Ochsenbein, S. T.; Murrie, M.; Rusanov, E.; Stoeckli-Evans, H.; Sekine, C.; Güdel, H. U. *Inorg. Chem.* **2002**, *41*, 5133.

(6) Yang, E. C.; Hendrickson, D. N.; Wernsdorfer, W.; Nakano, M.; Zakharov, L. N.; Sommer, R. D.; Rheingold, A. L.; Ledezma-Gairaud, M.; Christou, G. *J. Appl. Phys.* **2002**, *91*, 7382.

(7) Sun, Z. M.; Grant, C. M.; Castro, S. L.; Hendrickson, D. N.; Christou, G. *Chem. Commun.* **1998**, 721.

(8) (a) Osa, S.; Kido, T.; Matsumoto, M.; Re, N.; Pochaba, A.; Mrozinski, A. *J. Am. Chem. Soc.* **2004**, *126*, 420. (b) Zaleski, C. M.; Depperman, E. C.; Kampf, J. W.; Kirk, M. L.; Pecoraro, V. L. *Angew. Chem., Int. Ed.* **2004**, *43*, 3912. (c) Mishra, A.; Wernsdorfer, W.; Abboud, K. A.; Christou, G. *J. Am. Chem. Soc.* **2004**, *126*, 15648. (d) Mishra, A.; Wernsdorfer, W.; Parsons, S.; Christou, G.; Brechin, E. K. *Chem. Commun.* **2005**, 2086.

(9) (a) Winpenny, R. E. P. *Dalton Trans.* **2002**, 1. (b) Christou, G. *Polyhderon* **2005**, *24*, 2065. (c) Aromí, G.; Brechin, E. K. *Struct. Bonding* **2006**, *122*, 1.

(10) (a) Rebilly, J.-N.; Mallah, T. *Struct. Bonding* **2006**, *122*, 103. (b) Beltran, L. M. C.; Long, J. R. *Acc. Chem. Res.* **2005**, *38*, 325. (c) Parker, R. J.; Spiccia, L.; Berry, K. J.; Fallon, G. D.; Moubaraki, B.; Murray, K. S. *Chem. Commun.* **2001**, 333. (d) Marvaud, V.; Decroix, C.; Sculler, A.; Guyard-Duhayon, C.; Vaissermann, J.; Gonnet, F.; Verdaguer, M. *Chem.−Eur. J.* **2003**, *9*, 1677. (e) Marvaud, V.; Decroix, C.; Sculler, A.; Tuyeras, F.; Guyard-Duhayon, C.; Vaissermann, J.; Marrot, M.; Gonnet, F.; Verdaguer, M. *Chem.−Eur. J.* **2003**, *9*, 1692.

(11) (a) Murugesu, M.; Raftery, J.; Wernsdorfer, W.; Christou, G.; Brechin, E. K. *Inorg. Chem.* **2004**, *43*, 4203. (b) Rajaraman, G.; Murugesu, M.; Soler, M.; Wernsdorfer, W.; Helliwell, M.; Teat, S. J.; Christou, G.; Brechin, E. K. *J. Am. Chem. Soc.* **2004**, *126*, 15445. (c) Milios, C. J.; Fabbiani, F. P. A.; Parsons, S.; Murugesu, M.; Christou, G.; Brechin, E. K. *Dalton Trans.* **2005**, 351.

(12) (a) Vincent, J. B.; Chang, H. R.; Folting, K.; Huffman, J. C.; Christou, G.; Hendrickson, D. N. *J. Am. Chem. Soc.* **1987**, *109*, 5703. (b) Vincent, J. B.; Folting, K.; Huffman, J. C.; Christou, G. *Inorg. Chem.* **1986**, *25*, 996.

[Mn₆(acac)₄(OAc)₂(Htmp)₂(H₂N-ep)₂] (2). To a stirred suspension of Mn(acac)₂ (0.500 g, 1.97 mmol) in CH₃CN (30 mL) were added 1,1,1-tris(hydroxymethyl)ethane (H₃tmp;0.265 g, 1.97 mmol) and 2-amino-2-ethyl-1,3-propanediol (H₂N−H₂ep; 0.236 g, 1.97 mmol). The resulting yellow-brown suspension was left stirring overnight, during which time it changed to dark brown. The solution was filtered through Celite and left undisturbed to evaporate slowly. During 5 days, dark-brown crystals formed and were separated by filtration, washed with Et₂O, and dried in vacuo; yield ∼30%. Anal. Calcd (found) for [Mn₆(acac)₄(OAc)₂(Htmp)₂(H₂N-ep)₂] (**2**): C, 41.25 (41.36); H, 2.09 (2.20); N, 6.01 (6.12). Selected IR data (KBr disk, cm⁻¹): 1573vs, 1515vs, 1390vs, 1258m, 1196w, 1166w, 1064s, 1036m, 957m, 920m, 778m, 650w, 615s, 546s.

[Mn₆(OAc)₈(tmp)₂(py)₄]·2py (3·2py). Method 1. Treatment of a pale-pink solution of Mn(OAc)₂·4H₂O (0.245 g, 1.00 mmol) in py (25 mL) with NBu₄ⁿMnO₄ (0.120 g, 0.33 mmol) resulted in a dark-red-brown solution. To this solution was slowly added H₃-tmp (0.135 g, 1.00 mmol) followed by stirring for a further 45 min. The solution was filtered and layered with two volumes of Et₂O to give dark-brown crystals after a period of 3 days. The crystals were collected by filtration, washed with Et₂O, and dried in vacuo; yield ∼30%. A sample for X-ray crystallography was kept in the mother liquor to prevent solvent loss. Anal. Calcd (found) for [Mn₆(OAc)₈-(tmp)₂(py)₄] (**3**): C, 41.76 (41.67); H, 4.82 (4.74); N, 4.06 (3.99). Selected IR data (KBr disk, cm⁻¹): 1617s, 1578vs, 1436vs, 1335m, 1219w, 1113m, 1056m, 961m, 754w, 703s, 552m, 524m.

Method 2. To a stirred dark red-brown solution of [Mn₃O(OAc)₆-(py)₃]·py (0.425 g, 0.50 mmol) in py (25 mL) was added solid H₃tmp (0.405 g, 1.50 mmol). The solution was stirred for a period of 45 min, filtered, and then layered with two volumes of Et₂O, giving dark-brown crystals of **3**·2py after 3 days. The crystals were collected by filtration, washed with Et₂O, and dried in vacuo; yield ∼35%. The dried sample analyzed as solvent-free (**3**).

Method 3. Treatment of a dark-brown solution of [Mn₁₂O₁₂-(OAc)₁₆(H₂O)₄]·2AcOH·4H₂O (0.500 g, 0.25 mmol) in py (25 mL) with H₃tmp (0.203 g, 1.5 mmol) resulted in a solution of essentially the same color. The new solution was stirred vigorously for 45 min, filtered, and layered with two volumes of Et₂O, giving dark-brown crystals of **3**·2py after 2 days. The crystals were collected by filtration, washed with Et₂O, and dried in vacuo; yield ∼25%. The dried sample analyzed satisfactorily as solvent-free (**3**).

[Mn₆(OAc)₈(thme)₂(py)₄]·2py (4·2py). Method 1. Treatment of a pale-pink solution of Mn(OAc)₂·4H₂O (0.245 g, 1.00 mmol) in py (25 mL) with NBu₄ⁿMnO₄ (0.120 g, 0.33 mmol) resulted in the formation of a dark-purple-brown solution. To this solution was slowly added H₃thme (0.125 g, 1.00 mmol) to give a dark-brown solution, which was then left stirring for a further 45 min. The solution was then filtered and layered with two volumes of Et₂O, giving dark-brown crystals during 3 days. The crystals were collected by filtration, washed with Et₂O, and dried in vacuo; yield ∼35%. A sample for X-ray crystallography was kept in the mother liquor to prevent solvent loss. Anal. Calcd (found) for [Mn₆(OAc)₈-(thme)₂(py)₄] (**4**): C, 40.85 (40.96); H, 4.62 (4.71); N, 4.14 (4.20). Selected IR data (KBr disk, cm⁻¹): 1557vs, 1485w, 1418vs, 1338w, 1220w, 1122s, 1037vs, 758w, 704s, 661s, 617s, 524s.

Method 2. The synthesis of complex **3**·2py (method 2) was repeated using H₃thme (0.188 g, 1.5 mmol) in place of H₃tmp. This results in the formation of X-ray-quality dark-brown crystals of **4**·2py in approximately 35% yield. The dried sample analyzed satisfactorily as solvent-free (**4**).

Method 3. Method 3 for complex **3**·2py was repeated using H₃-thme (0.188 g, 1.5 mmol) in place of H₃tmp. This gives dark-brown

crystals of **5**·2py in a yield of ∼25%. The dried sample analyzed satisfactorily as solvent-free (**4**).

Physical Methods. Elemental analyses (C, H, and N) were performed by EastChem microanalysis service. IR spectra (4000−450 cm⁻¹) were recorded as KBr pellets on a Jasco FT/IR-410 spectrophotometer. Variable-temperature, solid-state direct current (dc) magnetic susceptibility data down to 1.80 K were collected on a Quantum Design MPMS-XL SQUID magnetometer equipped with a 7-T dc magnet at University of Florida. Diamagnetic corrections were applied to the observed paramagnetic susceptibilities using Pascal's constants. Magnetization versus field hysteresis and dc decay measurements at temperatures below 1.8 K were performed on single crystals using a micro-SQUID instrument.[13]

X-ray Crystallography and Structure Solution. Diffraction data were collected at 150 K on a Bruker Smart Apex CCD diffractometer equipped with an Oxford Cryosystems LT device. The structures were solved by direct methods (*SHELXS*) and refined by full-matrix least squares against F^2 (CRYSTALS).[14] All H atoms were placed geometrically and allowed to ride on their host atom, unless otherwise stated. For complex **2**, some disorder exists, which was treated by using two parts and refining the occupancies with a free variable to total 1. For complex **3**·2py, the C/N atoms of the solvate pyridine were identified by H-atom location. For complex **4**·2py, the H atoms were placed geometrically, refined subject to geometric restraints, and then constrained to ride on their host atoms. Crystallographic data are summarized in Table 1. Full details can be found in the CIF files: CCDC 604815−604818.

Results and Discussion

Synthesis. The reaction between Mn(acac)₂ and H₃tmp in the presence of H₃tea in CH₃CN gives complex **1**, which was crystallographically identified as **1**·2MeCN. The complex is mixed-valent containing four Mnᴵᴵ and two Mnᴵᴵᴵ ions. Given that the starting Mn source contains exclusively Mnᴵᴵ ions, it is apparent that the Mnᴵᴵᴵ ions are generated upon oxidation by atmospheric O₂, a process very common in Mn cluster chemistry. To our initial surprise, there were no β-diketonate ligands and six acetates in the product despite the starting material being Mn(acac)₂. The transformation of β-diketonates to carboxylates is in itself not surprising and has been seen in a number of other polynuclear cluster compounds,[15] but it is rare to find the conversion in 100% yield with no β-diketonates in the crystallized product (from a total yield of 35%; see the Experimental Section). The retro-Claisen condensation responsible is base-assisted, and here the excess H₃tea has clearly acted to mediate the reaction in high yield (vide infra).[16]

With the identity of complex **1** established and in an attempt to incorporate some acac⁻ ligands into the final

(13) Wernsdorfer, W. *Adv. Chem. Phys.* **2001**, *118*, 99.

(14) Betteridge, P. W.; Carruthers, J. R.; Cooper, R. I.; Prout, K.; Watkin, D. J. *J. Appl. Crystallogr.* **2003**, *36*, 1487.

(15) (a) Wang, S.; Pang, Z.; Smith, K. D. L.; Hua, Y.-S.; Deslippe, C.; Wagner, M. J. *Inorg. Chem.* **1995**, *34*, 908. (b) Drake, S. R.; Lyons, A.; Otway, D. J.; Williams, D. J. *Inorg. Chem.* **1994**, *33*, 1230. (c) Milios, C. J.; Kefalloniti, E.; Raptopoulou, C. P.; Terzis, A.; Vicente, R.; Perlepes, S. P. *Polyhedron* **2004**, *23*, 83. (d) Milios, C. J.; Kyritsis, P.; Raptopoulou, C. P.; Terzis, A.; Vicente, R.; Escuer, A.; Perlepes, S. P. *Dalton Trans.* **2005**, 501.

(16) (a) Bouwman, E.; Huffman, J. C.; Lobkovsky, E. B.; Christou, G. *Inorg. Chem.* **1992**, *31*, 4436. (b) Bouwman, E.; Caulton, K.; Christou, G.; Folting, K.; Gasser, C.; Hendrickson, D. N.; Huffman, J. C.; Lobkovsky, E. B.; Martin, J. D.; Michel, P.; Tsai, H.-L.; Xue, Z. *Inorg. Chem.* **1993**, *32*, 3463.

Table 1. Crystallographic Data for Complexes **1**−**4**

	1·2MeCN	**2**	**3·2py**	**4·2py**
formula[a]	$C_{40}H_{70}Mn_6N_4O_{24}$	$C_{46}H_{80}Mn_6N_2O_{22}$	$C_{58}H_{76}Mn_6N_6O_{22}$	$C_{56}H_{72}Mn_6N_6O_{22}$
M_w	1320.64	1342.76	1538.89	1510.78
cryst syst	monoclinic	monoclinic	triclinic	triclinic
space group	$C2/c$	$P2_1/n$	$P\bar{1}$	$P\bar{1}$
a/Å	18.4000(4)	11.8646(4)	11.5769(3)	11.3410(2)
b/Å	19.9266(5)	16.8058(6)	11.9600(3)	11.8770(2)
c/Å	15.8408(3)	14.7813(6)	14.2401(4)	13.7420(2)
α/deg	90	90	90.472(2)	79.7320(10)
β/deg	109.8460(10)	102.957	111.732(2)	66.1610(10)
γ/deg	90	90	110.1270(10)	74.4270(10)
V/Å^3	5463.1(2)	2872.26(18)	1698.77(8)	1625.82(5)
Z	4	2	1	1
T/K	150(2)	150(2)	150(2)	150(2)
λ^b/Å	0.71073	0.71073	0.71073	0.71073
D_c/g cm^{-3}	1.606	1.553	1.504	1.543
μ(Mo Ka)/ mm^{-1}	1.426	1.355	1.158	1.208
measd/indep (R_{int}) reflns	33047/7990 (0.0381)	34259/6283 (0.0940)	29001/9205 (0.0345)	43836/9566 (0.033)
obsd reflns [$I > 4\sigma(I)$]	7063	3989	7809	7252
wR2^{c,d}	0.1133	0.1233	0.0921	0.0726
R1^{d,e}	0.0488	0.0483	0.0349	0.0311
GOF on F^2	1.177	1.009	1.057	0.8517
$\Delta\rho_{max,min}$/e Å^{-3}	0.699, −0.522	0.707, −0.358	0.477, −0.445	0.53, −0.31

^{a} Including solvate molecules. ^{b} Mo Kα radiation, graphite monochromator. ^{c} wR2 = $[\sum w(|F_o^2| - |F_c^2|)^2/\sum w|F_o^2|^2]^{1/2}$. ^{d} For observed data. ^{e} R1 = $\sum ||F_o| - |F_c||/\sum|F_o|$.

product, we repeated the reaction using exactly the same reaction conditions (e.g., reaction time, concentrations, etc.) but replacing H₃tea (pK_a ∼ 13) with H₂N−H₂ep (pK_a ∼ 11). The result was the isolation of complex **2**, in which both acac⁻ and OAc⁻ ligands are present and where the acac⁻ to OAc⁻ transformation is 77% less than that observed for complex **1**. In addition, complex **2** contains only doubly deprotonated Htmp²⁻ ligands, while in complex **1**, both are fully deprotonated tmp³⁻, as might be expected by the use of a weaker base.

The syntheses of both complexes **3** and **4** can be regarded either as "reductive aggregations" or as comproportionations depending on the method used. Here, comproportionation is the simple reaction between a Mn^{II} salt [e.g., Mn(OAc)₂· 4H₂O] and a source of Mn^{VII} (e.g., NBu₄^{n}MnO₄), while reductive aggregation is a process whereby high-oxidation-state Mn sources are reacted in reducing conditions that force a reduction of the metal center(s) (e.g., Mn^{III} to Mn^{II}) and structural rearrangement (in the presence or absence of additional bridging ligands) that results in the formation of a new product. For example, complex **3** is made from the reaction of Mn(OAc)₂·4H₂O and NBu₄^{n}MnO₄ in pyridine in the presence of the tripodal bridging ligand H₃tmp. When mixed together, Mn(OAc)₂·4H₂O and NBu₄^{n}MnO₄ initially form a bright-purple solution, which then turns dark brown upon stirring as the Mn^{VII} ions are reduced and the Mn^{II} ions oxidized. At this stage, H₃tmp is added (to avoid ligand oxidation) with the deprotonation and complexation of the ligand accompanied by a further reduction in the metal oxidation states as the solution color turns (over several hours) light brown. Complex **4** can be made from the reaction of [Mn₁₂O₁₂(OAc)₁₆(H₂O)₄] with H₃thme; the [Mn₁₂] cluster contains Mn^{IV} and Mn^{III} ions and the tripodal ligand is added in its fully protonated form (H₃thme), yet the product contains a [Mn^{III}₂Mn^{II}₄] core held together by triply deprotonated thme³⁻ ligands. Clearly, as is the case with almost all Mn

cluster chemistry, complexes **1**−**4** are unlikely to be the only species present, and their formation and crystallization is an extremely complicated process that also involves the protonation/deprotonation, structural rearrangement, and redox chemistry of many other species present in solution.

The success of these comproportionation reactions also led us to attempt the synthesis of similar [Mn₆] complexes but in different oxidation levels, particularly those complexes with a higher Mn^{III}-to-Mn^{II} ratio. Reactions involving the use of greater ratios of MnO₄⁻ and in the presence of additional anions were examined in detail but resulted only in the formation of identical complexes, albeit in differing yields. Similarly, when the reductive aggregation route was employed by replacing the [Mn^{III}₃] triangles with higher oxidation state sources such as [Mn₁₂O₁₂(OAc)₁₆(H₂O)₄] (which comprises four Mn^{IV} and eight Mn^{III} ions), only the same products could be crystallized. The relatively high yields of these hexanuclear clusters and their ease of crystallization suggest their formation to be more thermodynamically favorable than that of any higher oxidation state analogue(s) that may also be present in solution.

Description of the Structures. The structure of complex **1** is shown in Figure 1 with selected bond lengths and angles given in Table 2. The core consists of a rodlike [Mn^{III}₂Mn^{II}₄-(μ_2-OR)₆(μ_3-OR)₄]$^{4+}$ unit comprising four edge-sharing triangles, with Mn1 and its symmetry equivalent being the sole Mn^{III} ions. All six Mn ions effectively lie on the same plane and are in distorted octahedral geometries, except for Mn3 and Mn3′, which can be considered as *pseudo*-seven-coordinate with a long contact to the N atom of the triethanolamine ligand [Mn3−N1B 2.523(1) Å]. The two Mn^{III} ions display the expected Jahn−Teller (JT) elongations [Mn1−O1D, 2.177(2) Å; Mn1−O2A′, 2.238(2) Å], which are coparallel and at an angle of ∼37° with respect to the central plane of the six Mn ions. The two tripodal alcohol ligands are fully deprotonated, tmp³⁻, and located directly
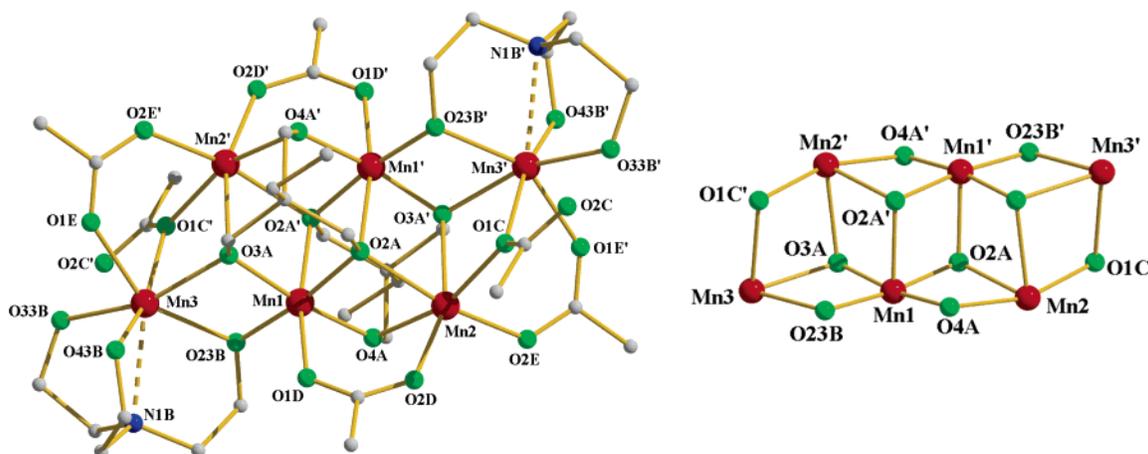
Figure 1. Molecular structure and core of complex **1** in the crystal. H atoms and solvent molecules have been omitted for clarity. Color code: red = Mn, green = O, blue = N, gray = C.

Table 2. Selected Interatomic Distances (Å) and Angles (deg) for **1·2MeCN**

Mn1−O2A	1.956(7)	Mn2−O2A	2.192(4)
Mn1−O2A′	2.238(5)	Mn2−O3A′	2.417(8)
Mn1−O3A	1.925(3)	Mn2−O4A	2.126(5)
Mn1−O4A	1.900(5)	Mn2−O1C	2.191(2)
Mn1−O23B	1.897(1)	Mn2−O2D	2.126(8)
Mn1−O1D	2.177(2)	Mn2−O2E	2.069(6)
Mn3−N1B	2.523(1)	Mn3−O33B	2.220(8)
Mn3−O23B	2.216(7)	Mn3−O43B	2.223(5)
Mn3−O1C′	2.427(5)	Mn3−O1E	2.184(2)
Mn3−O3A	2.245(3)		
Mn1−O2A−Mn2	95.3(2)	Mn1−O3A−Mn3	101.9(5)
Mn1−O2A′−Mn1′	99.2(7)	Mn1−O3A−Mn2′	100.9(9)
Mn2−O2A′−Mn1	98.8(5)	Mn3−O3A−Mn2′	93.3(2)
Mn1−O4A−Mn2	99.2(5)	Mn1−O23B−Mn3	103.9(7)
Mn2−O1C−Mn3′	94.4(2)		

above and below the [Mn_6] plane, each bonding in a η^3: η^3: η^2:μ_5 fashion to five metal centers that form three edge-sharing triangles. The six carboxylates coordinate in two different ways: four in the usual η^1:η^1:μ_2 mode and two in the monatomic μ_2 mode. The triethanolamine ligands are doubly protonated, H_2tea^-, capping each end of the molecule in a η^2:η^1:η^1:η^1:μ_2 mode. Both protonated arms of each H_2tea^- ligand are involved in H bonding; one arm forms an intermolecular H bond to an O atom of the monatomic acetate belonging to a neighboring [Mn_6] unit, while the second protonated arm forms an intramolecular H bond to the O atom of the monatomic acetate belonging to the same [Mn_6] unit.

The molecules in the crystal lattice stack directly upon each other, forming sheets, with the solvent molecules occupying the space within these sheets. The closest intermolecular Mn···Mn distance is 8.068(3) Å between adjacent sheets and 7.861(2) Å within the same sheet.

The structure of complex **2** is shown in Figure 2 with selected bond lengths and angles given in Table 3. The core of complex **2** consists of a rodlike planar [$Mn^{III}_2Mn^{II}_4(\mu_2$-OR)$_6(\mu_3$-OR)$_4$]$^{4+}$ unit comprising four edge-sharing triangles. The sole Mn^{III} ions (Mn1 and Mn1′) are located in the center of the core, with all six Mn ions lying in the same plane. All are six-coordinate, adopting distorted octahedral geometries and with the Mn^{III} ions displaying the expected JT elongations. These [Mn1−N21 2.308(2) Å; Mn1−O31′
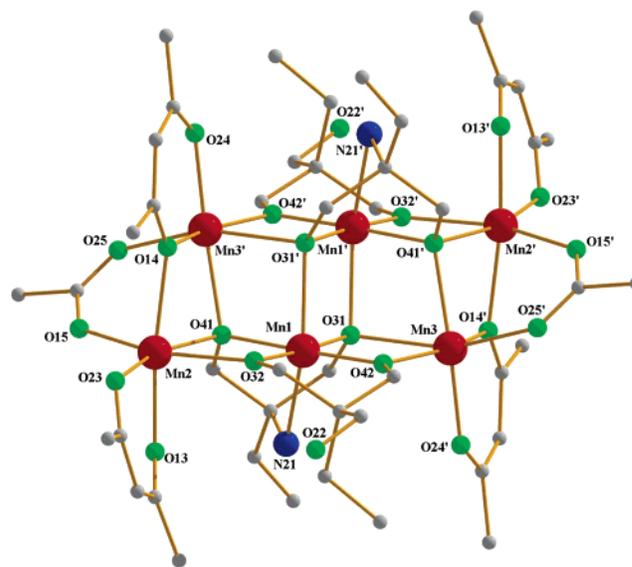

Figure 2. Molecular structure of complex **2**. H atoms have been omitted for clarity. The color code is the same as that in Figure 1.

Table 3. Selected Interatomic Distances (Å) and Angles (deg) for **2**

Mn1−O32	1.863(2)	Mn2−O23	2.085(2)
Mn1−O42	1.877(2)	Mn2−O13	2.139(3)
Mn1−O41	1.950(2)	Mn2−O15	2.177(2)
Mn1−O31	1.951(2)	Mn2−O32	2.206(2)
Mn1−O31′	2.260(2)	Mn2−O14	2.238(2)
Mn1−N21	2.308(3)	Mn2−O41	2.245(2)
Mn3−O24′	2.092(3)	Mn3−O25′	2.116(3)
Mn3−O42	2.133(2)	Mn3−O14′	2.166(2)
Mn3−O41′	2.229(2)	Mn3−O31	2.279(2)
Mn1−O31′−Mn1′	100.7(1)	Mn1−O41−Mn3′	107.6(4)
Mn1−O31′−Mn3′	97.0(7)	Mn1−O41−Mn2	99.4(1)
Mn1−O31−Mn3′	97.1(8)	Mn3′−O41−Mn2	93.8(5)
Mn1−O32−Mn2	103.5(9)	Mn1−O42−Mn3′	104.6(4)
Mn3−O14′−Mn2′	95.8(1)		

2.260(2) Å] are again coparallel and at an angle of ∼29° with respect to the central plane of the Mn ions.

The two tripodal alcohol ligands are doubly deprotonated, $Htmp^{2-}$, sitting above and below the [Mn_6] plane, coordinating via only two of their three arms in a η^2:η^2:μ_3 fashion linking three Mn ions together in a linear array. The two 2-amino-2-ethyl-1,3-propanediol ligands are doubly deprotonated, H_2N-ep^{2-}, lying above and below the [Mn_6] plane,
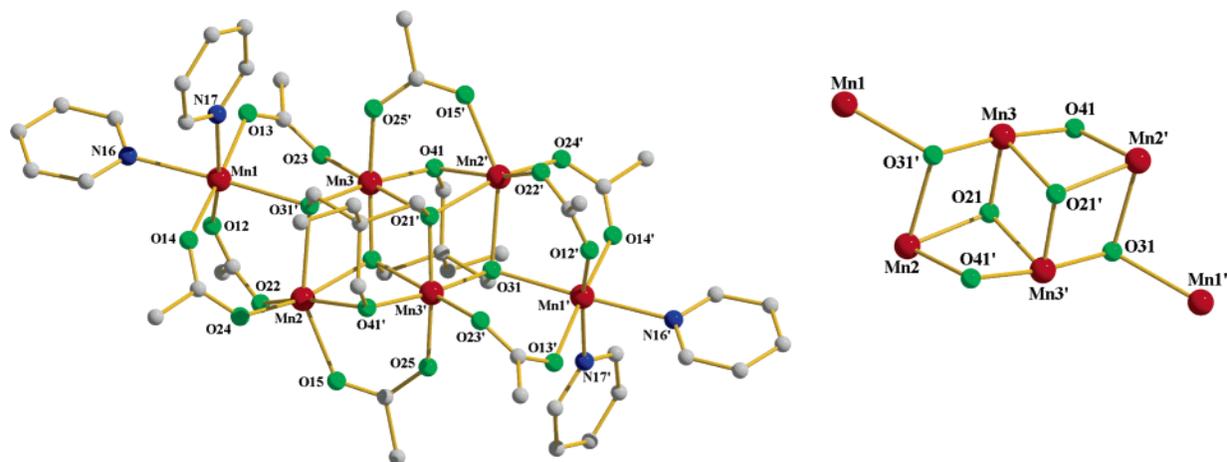
Figure 3. Molecular structure and core of complex **3**. H atoms and solvent molecules are omitted for clarity. The color code is the same as that in Figure 1.

Table 4. Selected Interatomic Distances (Å) and Angles (deg) for **3·2py**

Mn1−O12	2.125(1)	Mn2−O24	2.083(7)
Mn1−O14	2.132(1)	Mn2−O22	2.098(1)
Mn1−O13	2.136(2)	Mn2−O41′	2.164(1)
Mn1−N17	2.295(9)	Mn2−O21	2.202(6)
Mn1−N16	2.315(2)	Mn2−O15	2.207(2)
Mn1−O31′	2.378(1)	Mn2−O31′	2.353(5)
Mn3−O41	1.878(5)	Mn3−O25′	1.972(3)
Mn3−O21	1.943(1)	Mn3−O23	2.124(1)
Mn3−O31′	1.944(1)	Mn3−O21′	2.289(1)
Mn3−O21−Mn2	104.8(3)	Mn3′−O31−Mn2′	99.4(3)
Mn3−O21′−Mn3′	98.8(1)	Mn3′−O31−Mn1′	116.6(9)
Mn2−O21−Mn3′	89.5(1)	Mn2′−O31−Mn1′	96.6(7)
Mn3−O41−Mn2′	102.7(4)		

coordinating in a η^3:η^3:η^1:μ_5 mode to five metal centers that form three edge-sharing triangles. Two of the acac⁻ ligands adopt their common chelating mode, while the remaining two bond in the more unusual η^2:η^1:μ_2 fashion. The coordination spheres of the peripheral Mn ions are completed by the presence of η^1:η^1:μ_2-acetates that bridge between Mn2 and Mn3′ (and symmetry equivalents). The protonated OH group of the nondeprotonated arm of each Htmp²⁻ forms an intermolecular H bond to an O atom belonging to a bridging acetate of a neighboring [Mn₆] unit. As a result of these interactions, each [Mn₆] unit forms four H bonds (two from the Htmp²⁻ ligands and two from the bridging acetates) to four different neighboring [Mn₆] species belonging to the same sheet and, thus, the molecules form 2D sheets held together by a complicated network of H bonds. These 2D networks stack upon each other, leaving no solvent accessible void, with the closest Mn···Mn distance in the same sheet of 8.483(2) Å and a distance of 7.621(2) Å between adjacent sheets.

Complex **3** is shown in Figure 3 with selected distances and angles given in Table 4. Its core can be described as a nonplanar [Mnᴵᴵᴵ₂Mnᴵᴵ₄(μ_2-OR)₂(μ_3-OR)₄]⁸⁺ unit, or again more conveniently as a central planar [Mnᴵᴵᴵ₂Mnᴵᴵ₂] rhomb (comprising Mn2, Mn2′, Mn3, and Mn3′) with two peripheral Mn ions (Mn1 and Mn1′) above and below the plane at distances of 1.107(3) and 1.107(3) Å, respectively. The two Mnᴵᴵᴵ ions are Mn3 and Mn3′ with their JT elongations described by the Mn3−O23 [2.124(2) Å] and Mn3−O21′ [2.289(1) Å] directions at an angle of ∼57° with respect to

the [Mn₄] plane. The tripodal alcohols are fully deprotonated, tmp³⁻, sitting one above and one below the [Mn₄] plane, coordinating in a η^3:η^3:η^2:μ_5 fashion bridging five metals to form three edge-sharing triangles. All eight acetates adopt a η^1:η^1:μ_2 bridging mode, while the coordination environment of the peripheral Mn ions is completed by four terminal pyridine ligands. In the crystal lattice, the molecules pack upon each other, forming sheets with the pyridine solvate molecules lying in the space between adjacent sheets. There are no intermolecular or intramolecular H bonds present between [Mn₆] units, while the closest Mn···Mn distance is 7.688(2) Å.

Complex **4** is shown in Figure 4 with selected bond lengths and angles given in Table 5. The core of the complex consists of a nonplanar [Mnᴵᴵᴵ₂Mnᴵᴵ₄(μ_2-OR)₄(μ_3-OR)₄]⁶⁺ unit and can be described as consisting of a central [Mnᴵᴵᴵ₂Mnᴵᴵ] plane (comprising Mn2, Mn2′, Mn3, and Mn3′) with two Mn ions (Mn1 and Mn1′) located above and below the plane at distances of 1.167(1) and 1.167(1) Å, respectively. The two central Mnᴵᴵᴵ ions (Mn3 and Mn3′) have JT elongations described by Mn3−O14 [2.148(1) Å] and Mn3−O21′ [2.303(1) Å] at an angle of ∼57° with respect to the [Mn₄] plane, similar to that seen in complex **3**. All of the Mn ions are six-coordinate, adopting distorted octahedral geometries, with the exception of Mn2, which is *pseudo*-seven-coordinate, displaying a long contact to the unbound O atom of a carboxylate ligand [Mn2−O22 2.818(2) Å]. The tripodal alcohols are fully deprotonated, thme³⁻, each coordinating in a η^3:η^3:η^2:μ_5 fashion bridging five metals. The acetates adopt two different coordination modes: six are in the usual η^1:η^1:μ_2 mode, while the remaining are η^2:η^1:μ_2. The coordination sphere of the peripheral Mn ion (Mn1) is completed by two terminal pyridine ligands. In the crystal, each [Mn₆] complex sits directly on top of another, creating a column of [Mn₆] molecules encapsulating the pyridine solvate molecules, with the closest contacts in this direction being between the terminal pyridine ligands and the solvate pyridine molecules at 3.766(3) Å, while in the perpendicular direction the closest contact is between the methyl groups of the bridging acetates at 5.510(2) Å. The closest intermolecular Mn···Mn distance is 9.207(2) Å.
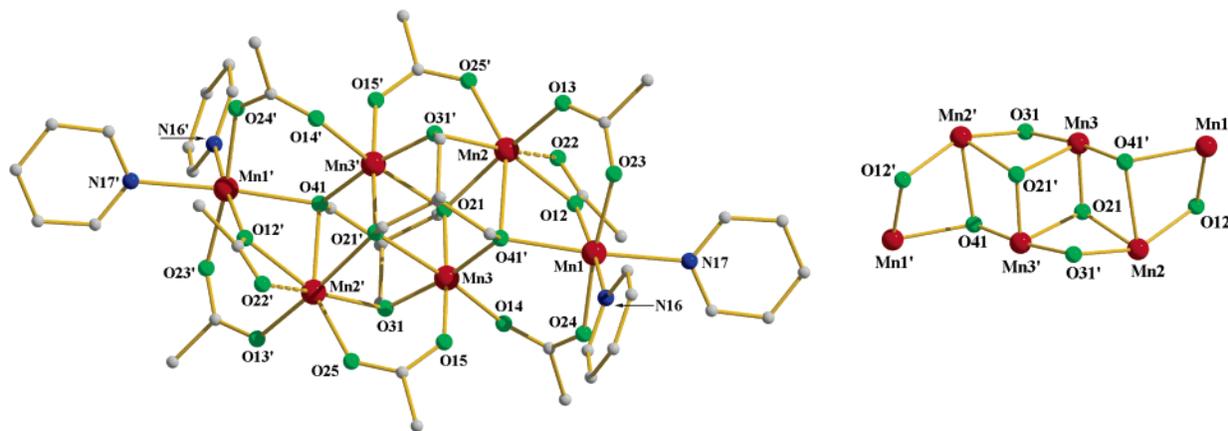
Figure 4. Molecular structure and core of complex **4**. H atoms and solvent molecules are omitted for clarity. The color code is the same as that in Figure 1.

Table 5. Selected Interatomic Distances (Å) and Angles (deg) for **4·2py**

Mn1–O41′	2.265(1)	Mn2–O31′	2.174(7)
Mn1–O12	2.136(3)	Mn2–O25′	2.163(5)
Mn1–O23	2.162(8)	Mn2–O41′	2.509(2)
Mn1–O24	2.123(8)	Mn2–O21	2.187(5)
Mn1–N16	2.278(3)	Mn2–O22	2.818(2)
Mn1–N17	2.303(1)	Mn2–O12	2.172(7)
Mn3–O21	2.303(1)	Mn2–O13	2.095(1)
Mn3–O41′	1.934(1)	Mn3–O31	1.881(5)
Mn3–O21′	1.947(7)	Mn3–O14	2.148(5)
Mn3–O15	1.973(5)		
Mn2–O21–Mn3′	90.3(1)	Mn2′–O31–Mn3	103.2(5)
Mn2–O21–Mn3	108.2(6)	Mn1′–O41–Mn3′	118.9(4)
Mn3′–O21′–Mn3	97.6(7)	Mn1′–O41–Mn2′	89.6(2)
Mn3′–O41–Mn2′	97.1(7)	Mn2′–O12′–Mn1′	102.8(7)
Mn2–O12–Mn1	102.8(7)		

Table 6. Bond Angles for the Central Planar $\{Mn^{III}_2Mn^{II}_2(\mu_2\text{-OR})_4(\mu_3\text{-OR})_2\}$ Rhomb Present in **1–4**

	angles (deg)				
complex	a	b	c	d	e
1	99.1(2)	95.5(1)	98.7(3)	100.9(1)	98.1(1)
2	100.7(1)	97.07(1)	96.1(2)	107.6(3)	104.6(1)
3	98.8(1)	89.5(1)	104.8(1)	99.4(3)	102.7(3)
4	97.6(1)	90.3(1)	108.2(6)	97.1(7)	103.2(4)

Table 7. BVS Calculations for Complexes **1–4**

	complex **1**				complex **2**			
	Mn^{2+}	Mn^{3+}	Mn^{4+}	ox.	Mn^{2+}	Mn^{3+}	Mn^{4+}	ox.
Mn1	3.47	3.20	3.14	3+	3.48	3.22	3.158	3+
Mn2	2.13	1.97	1.93	2+	2.12	1.95	1.92	2+
Mn3	1.75	1.62	1.59	2+	2.19	2.02	1.98	2+

	complex **3**				complex **4**			
	Mn^{2+}	Mn^{3+}	Mn^{4+}	ox.	Mn^{2+}	Mn^{3+}	Mn^{4+}	ox.
Mn1	1.97	1.85	1.81	2+	2.05	1.96	1.88	2+
Mn2	2.12	1.96	1.92	2+	2.00	1.84	1.81	2+
Mn3	3.39	3.12	3.06	3+	3.35	3.09	3.03	3+

In all cases, the oxidation states of the metal ions were assigned using a combination of charge-balance and bond-length considerations and bond valence sum (BVS) calculations (Table 7). The structures of complexes **1–4** are clearly related (Figure 5). All four consist of four edge-sharing [Mn$_3$] triangles that form "rods" of 8.45, 8.38, 9.23, and 8.96 Å in length, respectively. For complexes **3** and **4**, the two peripheral Mn ions lie above and below the plane described

by the four central Mn ions, while for **1** and **2**, all six Mn ions lie on the same plane. The metal topology in each case may be considered to be directed by the presence of the two μ_5-tripodal ligands that sit directly above and below the metal plane (Figure 5). Although the central $\{Mn^{III}_2Mn^{II}_2(\mu_2\text{-OR})_4$-$(\mu_3\text{-OR})_2\}$ rhomb present in all complexes **1–4** is planar, there are some subtle differences in the Mn–O–Mn angles (Chart 2 and Table 6) in this unit that are crucial for the magnetic behavior of the complexes (vide infra). Although there is no obvious trend, complexes **3** and **4** (in general) display smaller a, b, and d angles and larger c and e angles. The [Mn$^{III}_2$Mn$^{II}_2$] rhomb is connected to the two peripheral Mn^{II} ions in different ways in **1–4**: via only one μ_3-O atom in complex **3**, via one μ_3-O atom and one μ_2-O atom in complex **4**, and via one μ_3-O atom and two μ_2-O atoms in complexes **1** and **2** (Figure 5).

This planar diamond $\{Mn^{III}_2Mn^{II}_2(\mu_2\text{-OR})_4(\mu_3\text{-OR})_2\}$ core is rather common in manganese carboxylate chemistry and has been previously reported in the tetranuclear complexes [Mn$^{III}_2$Mn$^{II}_2$(hmp)$_6$(NO$_3$)$_2$(MeCN)$_2$]$^{2+}$ (**5**), [Mn$^{III}_2$Mn$^{II}_2$(hmp)$_6$-(NO$_3$)$_4$] (**6**), [Mn$^{III}_2$Mn$^{II}_2$(hmp)$_4$(acac)$_2$(MeO)$_2$]$^{2+}$ (**7**),[18] [Mn$^{III}_2$-Mn$^{II}_2$(O$_2$CMe)$_2$(pdmH)$_6$]$^{2+}$ (**8**),[19] [Mn$^{III}_2$Mn$^{II}_2$Br$_2$(hmp)$_6$-(H$_2$O)$_2$]$^{2+}$ (**9**),[20] [Mn$^{III}_2$Mn$^{II}_2$(O$_2$CMe)$_2$(LH)$_2$(LH$_2$)$_2$(H$_2$O)$_2$]$^{2+}$ (**10**),[21] [Mn$^{III}_2$Mn$^{II}_2$(O$_2$CPh)$_2$(LH)$_2$(LH$_2$)$_2$(H$_2$O)$_2$]$^{2+}$ (**11**),[21] and [Mn$^{III}_2$Mn$^{II}_2$(O$_2$CEt)$_2$(LH)$_2$(LH$_2$)$_2$(H$_2$O)$_2$]$^{2+}$ (**12**)[21] [where hmpH = 2-(hydroxymethyl)pyridine; pdmH$_2$ = pyridine-2,6-dimethanol; LH$_3$ = triethanolamine]; in the heptanuclear complex [Mn$^{III}_5$Mn$^{II}_2$(PhCO$_2$)$_9$(thme)$_2$(py)$_3$] (**13**);[11b] in the octanuclear complex [Mn$^{III}_4$Mn$^{II}_4$((CH$_3$)$_3$CCO$_2$)$_2$(tmp)$_2$(Htmp)$_4$-Br$_4$(H$_2$O)$_2$] (**14**);[11c] and in the dodecanuclear complex [Mn$^{III}_{10}$Mn$^{II}_2$O$_4$(OH)$_2$(PhCO$_2$)$_{12}$(thme)$_4$(py)$_2$] (**15**).[11b] The

(17) (a) Thorp, H. H. *Inorg. Chem.* **1992**, *31*, 1585. (b) Liu, W.; Thorp, H. H. *Inorg. Chem.* **1993**, *32*, 4102.
(18) Yang, E. C.; Harden, N.; Wernsdorfer, W.; Zakharov, L.; Brechin, E. K.; Rheingold, A. L.; Christou, G. *Polyhedron* **2003**, *22*, 1857.
(19) Yoo, J.; Brechin, E. K.; Yamaguchi, A.; Nakano, M.; Huffmann, J. C.; Maniero, A. L.; Brunel, L.-C.; Awaga, K.; Ishimoto, H.; Christou, G.; Hendrickson, D. N. *Inorg. Chem.* **2000**, *39*, 3615.
(20) Yoo, J.; Yamaguchi, A.; Nakano, M.; Krzystek, J.; Streib, W.; Brunel, L. C.; Ishimoto, H.; Christou, G.; Hendrickson, D. N. *Inorg. Chem.* **2001**, *40*, 4604.
(21) (a) Wittick, L. M.; Murray, K. S.; Moubaraki, B.; Batten, S. R.; Spiccia, L.; Berry, J. K. *Dalton Trans.* **2004**, 1003. (b) Wittick, L. M.; Jones, L. F.; Jensen, P.; Moubaraki, B.; Spiccia, L.; Berry, K. J.; Keith, S.; Murray, *Dalton Trans.* **2006**, 1534.
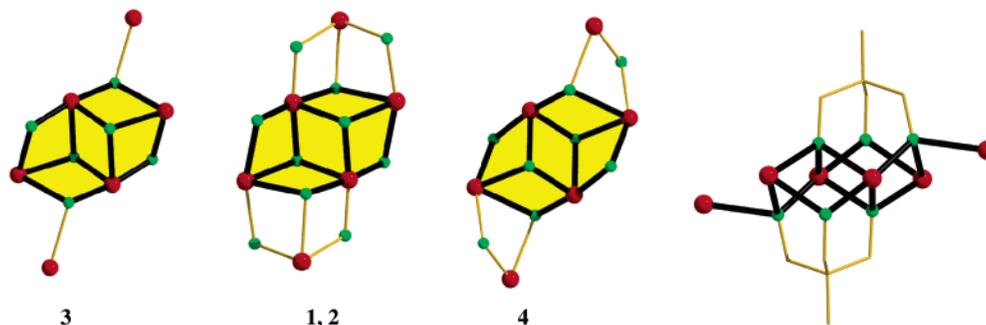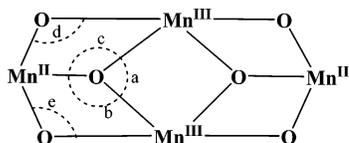
Figure 5. Comparison of the metal−oxygen cores of complexes **1**−**4** (left) and the μ_5-coordination mode of the central tripodal ligands (right). The color code is the same as that in Figure 1.

Chart 2. Structure of the Central $\{Mn^{III}_2Mn^{II}_2(\mu_2\text{-OR})_4(\mu_3\text{-OR})_2\}$ Planar Rhomb Common to Complexes **1**−**4**

$[Mn^{III}_2Mn^{II}_4(\mu_2\text{-OR})_6(\mu_3\text{-OR})_4]^{4+}$ core of complexes **1** and **2** has been seen previously in the hexanuclear complex $[Mn^{III}_2\text{-}Mn^{II}_4(CH_3CO_2)_6(thme)_2(H_2tea)_2]$ (**16**),[11b] while the $[Mn^{III}_2\text{-}Mn^{II}_4(\mu_2\text{-OR})_4(\mu_3\text{-OR})_4]^{6+}$ core of **4** has been previously reported in the complex $[Mn^{III}_2Mn^{II}_4((CH_3)_3CCO_2)_8(tmp)_2\text{-}(py)_2]$ (**17**).[11b] However, to the best of our knowledge, the $[Mn^{III}_2Mn^{II}_2(\mu_2\text{-OR})_2(\mu_3\text{-OR})_4]^{8+}$ topology of complex **3** is observed for the first time. "Reverse" rhomboidal clusters with $\{Mn^{II}_2Mn^{III}_3O_x\}$ (x = 2 and 3) cores in which the Mn^{III} ions are the wing tips and the Mn^{II} ions are the body ions have also been reported.[21b]

dc Magnetic Susceptibility Studies. dc magnetic susceptibility studies were performed on polycrystalline samples of complexes **1**−**4** in the 5−300 K range in an applied field of 0.1 T. The results are plotted as the $\chi_M T$ product vs T in Figure 6. The $\chi_M T$ values at 300 K are 24.20, 26.72, 23.49, and 23.10 cm³ K mol⁻¹ for **1**−**4**, respectively, close to the spin-only (g = 2) value of 23.5 cm³ K mol⁻¹ expected for a [Mn₆] unit comprising two high-spin Mn^{III} and four high-spin Mn^{II} ions. For complexes **1** and **2**, their $\chi_M T$ values remain essentially constant as the temperature decreases until ca. 50 K when they decrease rapidly to values of 6.02 and 3.84 cm³ K mol⁻¹ at 5 K, respectively. For complexes **3** and **4**, the room temperature $\chi_M T$ values of 23.49 and 23.10 cm³ K mol⁻¹ decrease gradually as the temperature decreases until ca. 125 K, when they both begin to decrease more rapidly and steadily to values 7.56 and 9.42 cm³ K mol⁻¹ at 5 K, respectively. This behavior is consistent with the presence of dominant antiferromagnetic interactions between the metal centers, with the low-temperature values indicating relatively small (S ≤ 4) spin ground states for all four complexes.

To determine the ground state of complexes **1**−**4**, variable-temperature, variable-field dc magnetization data were collected in the ranges 1.8−10 K and 0.1−7 T. The data were fitted by a matrix-diagonalization method to a model that assumes that only the ground state is populated, includes axial zero-field splitting ($D\hat{S}_z^2$), and carries out a full powder
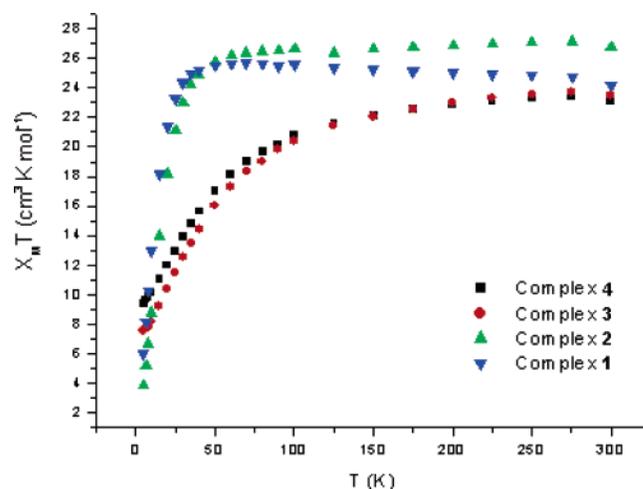

Figure 6. Plot of $\chi_M T$ vs T for complexes **1**−**4** in the 5−300 K temperature range in a field of 0.1 T.

average.[22] The corresponding Hamiltonian is given by

$$\hat{H} = D\hat{S}_z^2 + g\mu_B\mu_0\hat{S}_z H_z \tag{1}$$

where D is the axial anisotropy, μ_B is the Bohr magneton, μ_0 is the vacuum permeability, $\hat{S}_z$ is the easy-axis spin operator, and H_z is the applied field.

For complexes **1** and **2**, no satisfactory fit of the data was possible because the magnetization rises almost linearly with the applied magnetic field, indicating the existence of small (S ≈ 0) spin ground states with the presence of many low-lying excited states of larger multiplicity that become populated with increasing field. Low-lying excited states are a common problem in large clusters, particularly when there are multiple Mn^{II} ions present, as is the case here, because these give weak exchange interactions. The data for complexes **3** and **4** are plotted as reduced magnetization ($M/N\mu_B$) vs H/T in Figure 7. The best fits [obtained using only the low-field data (≤4 T)] gave S = 4, g = 1.82, and D = −0.44 cm⁻¹ for complex **3** and S = 4, g = 1.97, and D = −0.58 cm⁻¹ for complex **4**. When fields up to 7 T were employed, a poorer quality fit was obtained. This is characteristic of low-lying excited states with S values greater than the ground state of S = 4.

ac Magnetic Susceptibility Studies. ac susceptibility measurements were performed on complexes **1**−**4** in the

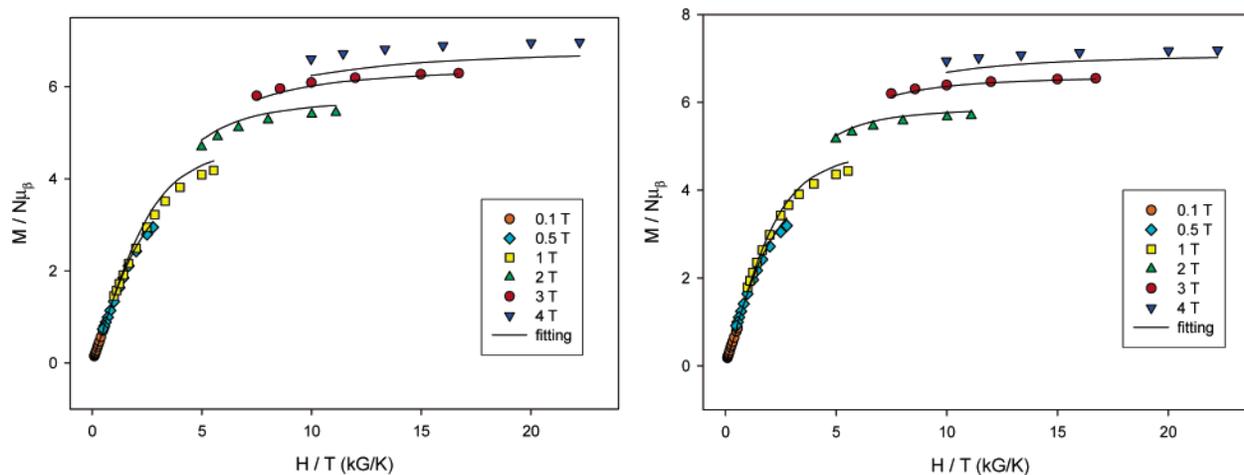(22) Davidson, E. R. MAGNET, Indiana University.

Figure 7. Magnetization data plotted as reduced magnetization ($M/N\mu_B$) vs H/T for complexes **3** (left) and **4** (right) in the ranges 0.1−4 T and 1.8−6 K.

1.8−10 K range in zero applied dc field and a 3.5 G ac field oscillating at 50−1300 Hz. For complexes **1** and **2**, extrapolation of the in-phase $\chi_M'T$ signal to 0 K suggests the existence of $S = 0$ spin ground states. In addition, the slopes of the plots all decrease rapidly with a decrease in the temperature, revealing the presence of several spin states of larger S values lying very close to the ground state, consistent with the dc data.

For complexes **3** and **4**, frequency-dependent out-of-phase (χ_M'') ac susceptibility signals are seen below approximately 2.5 K, but no peaks are observed and the magnitudes of the signals are small (Figure 8; for well-established SMMs, χ_M'' and $\chi_M'T$ are roughly of the same order of magnitude). For **3**, the in-phase $\chi_M'T$ signal increases slightly with a decrease in the temperature, while for **4**, the signal decreases. This is consistent with the presence of excited states with smaller and larger S values, respectively. The magnitudes of the in-phase $\chi_M'T$ vs T signals support the assignment of $S = 4$ ground states for both complexes.

Single-Crystal Hysteresis Studies. The S and D values obtained above for **3** and **4** suggest that these complexes may exhibit single-molecule magnetism behavior, with upper limits to the potential energy barrier (U) to magnetization reversal of $U = S^2|D| \approx 7.0$ cm^{-1} (~10 K) and 9.3 cm^{-1} (~13 K), respectively. To probe the possible SMM behavior further, single-crystal hysteresis loop and relaxation measurements were performed using a micro-SQUID setup.[23] Figures 9 and 10 present typical magnetization (M) vs applied dc field (H) measurements at different temperatures and scan rates with the field applied in the direction of the easy axis; the applied magnetic field was swept between −1 and +1 T.

For complex **3**, the data obtained at 40 mK show hysteresis loops with a very large step at zero field (Figure 9). A step indicates the occurrence of rapid relaxation of the magnetization at a given magnetic field where a level crossing is avoided. At $H = -1$ T, all of the molecules are in the $M_S = +4$ state. When the field is swept in a positive direction, there is resonance between the +4 and −4 M_S levels at $H =$
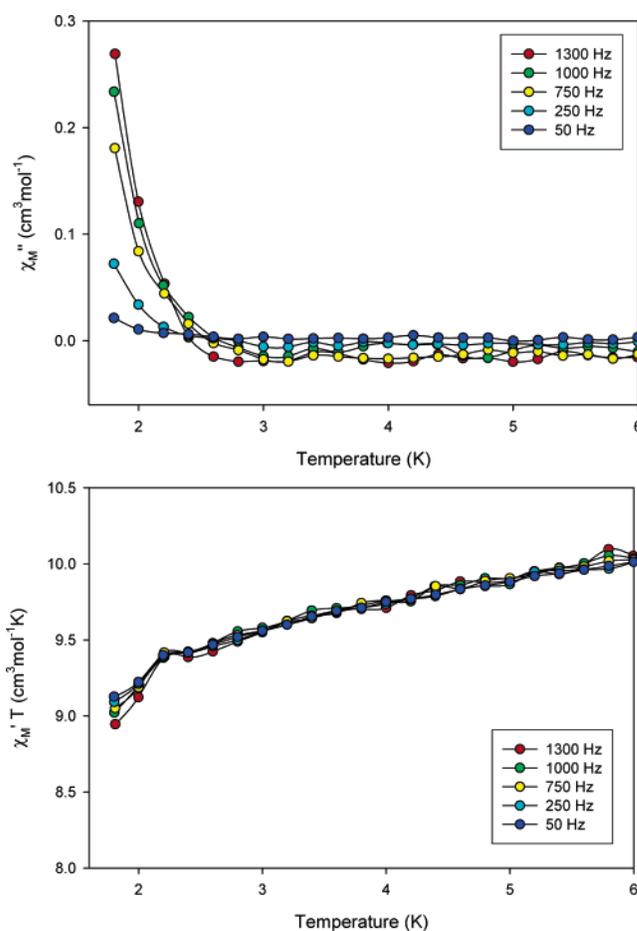

Figure 8. Plots of the in-phase (χ_M') signal as $\chi_M'T$ and out-of-phase (χ_M'') signal in ac susceptibility studies vs temperature in a 3.5-G field oscillating at the indicated frequencies for complex **4**.

0, and part of the molecules tunnel. The height of the step, in this case, indicates that the tunneling process is relatively fast. Upon an increase in the field above zero, another step corresponding to the molecules tunneling from the $M_S = +4$ to the $M_S = -3$ sublevel should occur at $H \approx D/g\mu_B$. However, for systems with relatively large tunnel splittings such as complex **3**, a direct relaxation process between the $M_S = +4$ ground-state levels becomes possible. This leads

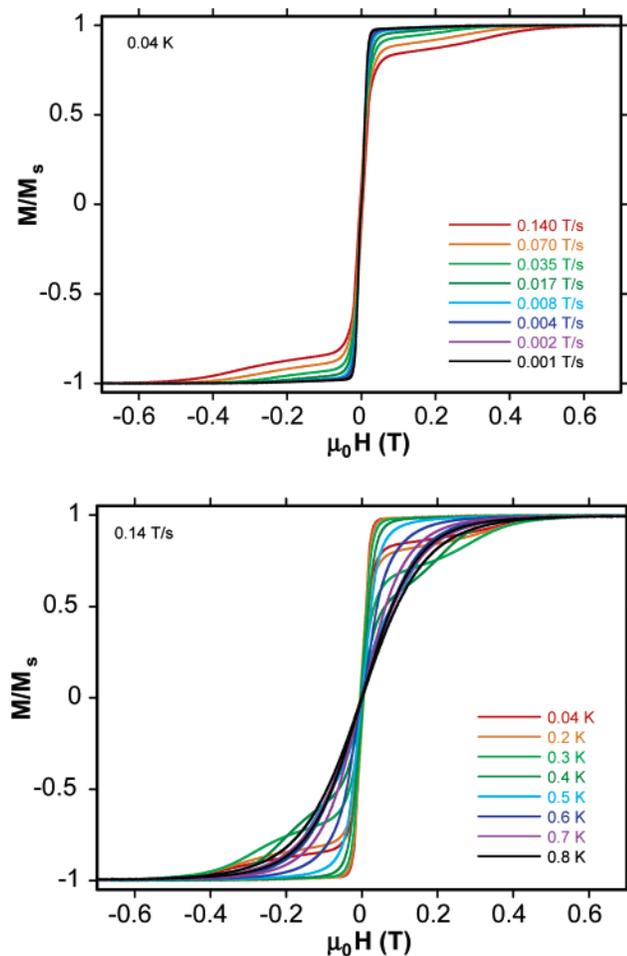(23) Wernsdorfer, W. *Adv. Chem. Phys.* **2001**, *118*, 99.

Figure 9. Single-crystal magnetization (*M*) of **3** vs applied magnetic field (*H*). The magnetization is normalized to its saturation value. The resulting hysteresis loops are shown at different temperatures and field sweep rates.

to a smeared step, which is further broadened by very weak intermolecular interactions (exchange and dipolar). When the same experiment is carried out at higher field sweep rates (Figure 9), the number of molecules tunneling at zero field decreases and the hysteresis loop is larger. In the variable-temperature experiment, hysteresis loops appear below ca. $T = 0.4$ K, indicating that below this temperature the magnetization is blocked. As the temperature is decreased, the number of molecules that undergo relaxation by thermal activation also decreases and those relaxing by tunneling increase, resulting in a narrowing of the hysteresis loop with a sharper step at $H = 0$.

Complex **4** shows similar behavior but with the blocking of the magnetization appearing below approximately 0.7 K and a pronounced sweep rate dependence (Figure 10). In the 40 mK plot, there are clear steps at ca. ±0.56 and ±0.7 T. We used minor hysteresis loops (inset of Figure 10) to assign these steps.[24] The step at ±0.7 T is due to tunneling from the $M_S = +4$ to the $M_S = -3$ sublevel, and the step at ±0.56 T is due to spin—spin cross-relaxation (SSCR).[25] This

(24) Wernsdorfer, W.; Bhaduri, S.; Vinslava, A.; Christou, G. *Phys. Rev. B* **2005**, *72*, 214429.
(25) Wernsdorfer, W.; Bhaduri, S.; Tiron, R.; Hendrickson, D. N.; Christou, G. *Phys. Rev. Lett.* **2002**, *89*, 197201.
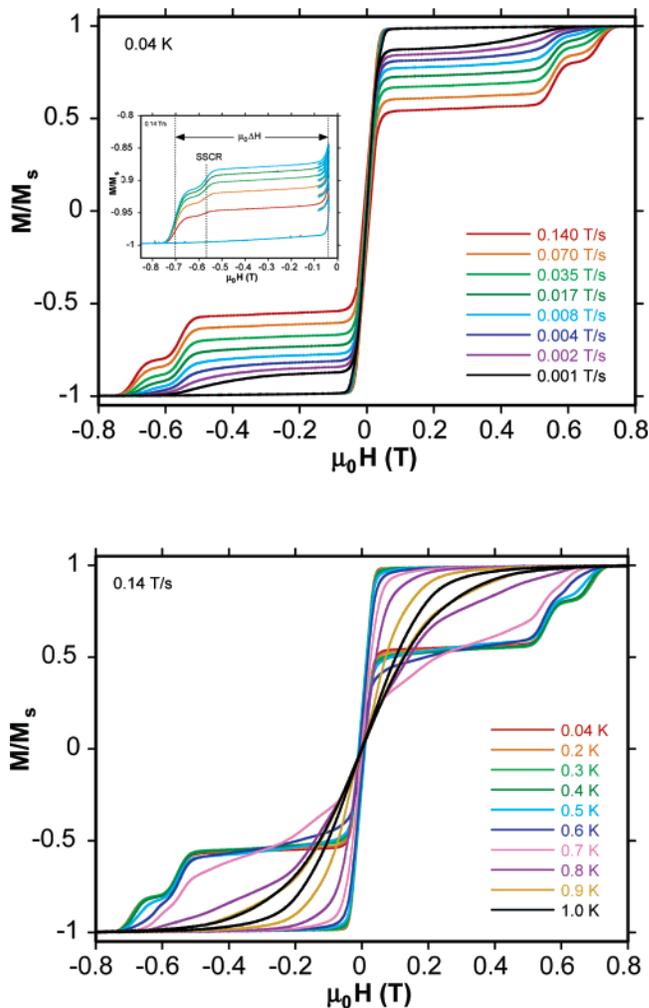
Figure 10. Single-crystal magnetization (*M*) of **4** vs applied magnetic field (*H*). The magnetization is normalized to its saturation value. The resulting hysteresis loops are shown at different temperatures and field sweep rates.

phenomenon is the result of weak dipolar and intermolecular exchange interactions between two (or more) SMMs in the crystal. A transition (i.e., one molecule transferring to a lower energy state and one to a higher energy state) can occur if SMMs are coupled because the transverse terms of the interaction allow a tunnel splitting between two quantum states. It is important to note that SSCR occurs in almost all SMMs but is often covered by other effects such as, for example, the direct relaxation processes for compound **3**.

Theoretical Studies. The calculation of magnetic exchange interactions between metal centers using density functional theory (DFT) is a new and appealing approach. In earlier decades, several qualitative models were proposed to calculate the exchange interactions in dinuclear complexes and two important models were widely employed: the Hey—Thibeault—Hoffmann model[26] and the Kahn model.[27] However, both used several approximations such as the active electron approximation, whereby only the unpaired electrons of the metal are taken into account while the contributions

(26) Hey, P. J.; Thibeault, J. C.; Hoffmann, R. *J. Am. Chem. Soc.* **1975**, *17*, 4884.
(27) Kahn, O. *Molecular Magnetism*; VCH Publishers: New York, 1993.

from core electrons are ignored, and subsequently both models did not provide good estimates of the J values compared to experiment. Later, Noodleman developed the broken-symmetry model based on nonorthogonal magnetic orbitals, which has proven to yield good numerical estimates of the J constant, even for very large systems.[28-30] The exchange interaction can be evaluated from the energy difference between the high-spin state and the broken-symmetry state using the following expression:[29]

$$J = \frac{2(E_{BS} - E_{HS})}{S_{HS}(S_{HS} + 1)} \quad (2)$$

where E_{HS} stands for the energy of high-spin state, E_{BS} stands for the energy of the broken-symmetry state, and S_{HS} is the spin on the metal centers. This method has recently been successfully extended to encompass polynuclear complexes by Alvarez and co-workers, who proposed a pairwise interaction model to calculate the magnetic exchange interactions.[29-32]

Here we have employed the same approach to calculate the five different exchange interactions present in complexes **1–4**. Although all are structurally very similar, being hexanuclear and presenting the same central {Mn$^{III}_2$Mn$^{II}_2$-(OR)$_6$} core and with only small differences in bond lengths and angles, they display remarkably different magnetic properties: complexes **1** and **2** have diamagnetic spin ground states, while **3** and **4** are SMMs. DFT calculations were performed using the B3LYP functional with Ahlrich's triple-ζ-quality basis set on the metal atoms and a double-ζ-quality basis set on the others. All of the calculations have been performed with the *Jaguar* (version 5.0) program.[33]

The five different exchange interactions in **1–4** are illustrated in Figure 11. The structural cores are similar to those of the family of Mn compounds reported previously by us, and therefore the same calculation procedure has been adopted here to compute the magnetic exchange interactions.[11b] The structures can be broken down into three different types: complexes **1** and **2**, complex **3**, and complex **4** (Figure 5), and the calculations have been performed on the crystal structures of **2–4**. The bridging units that mediate the exchange between the metal centers and their important structural parameters together with the DFT-calculated J
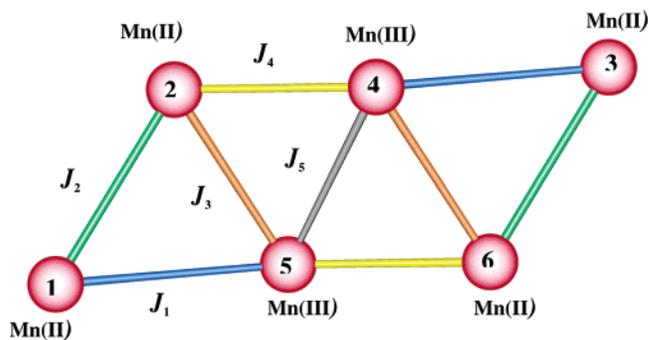
(28) Noodleman, L. *J. Chem. Phys.* **1981**, *74*, 5737.
(29) Ruiz, E.; Alvarez, S.; Rodriguez-Fortea, A.; Alemany, P.; Pouillon, Y.; Massobiro, C. In *Magnetism: Molecules to Materials II*; Miller, J. S., Drillon, M., Eds.; Wiley-VCH: Weinheim, Germany, 2001; p 227.
(30) (a) Abu-Nawwas, A. H.; Cano, J.; Christian, P.; Mallah, T.; Rajaraman, G.; Teat, S. J.; Winpenny, R. E. P.; Yukawa, Y. *Chem. Commun.* **2004**, 314. (b) Rajaraman, G.; Sañudo, E. C.; Helliwell, M.; Piligkos, S.; Wernsdorfer, W.; Christou, G.; Brechin, E. K. *Polyhedron* **2005**, *24*, 2450.
(31) Ruiz, E.; Cano, J.; Alvarez, S.; Caneschi, A.; Gatteschi, D. *J. Am. Chem. Soc.* **2003**, *152*, 6791.
(32) (a) Ruiz, E.; Rajaraman, G.; Alvarez, S.; Gillon, B.; Stride, J.; Clerac, R.; Larionova, L.; Decurtins, S. *Angew. Chem., Int. Ed.* **2005**, *117*, 2771. (b) Rajaraman, G.; Christensen, K. E.; Larsen, F. K.; Timco, G. A.; Winpenny, R. E. P. *Chem. Commun.* **2005**, 3053. (c) Rajaraman, G.; Cano, J.; Brechin, K. E.; McInness, E. J. L. *Chem. Commun.* **2004**, 1476.
(33) *Jaguar*, version 5.0: Schrodinger Inc.: Portland, OR, 2003.

Figure 11. Five different exchange interactions present in complexes **1–4**.

constants are given in Table 8. For complex **2**, the strong interactions are J_1, J_2, and J_5 and all are antiferromagnetic in nature. J_3 is calculated to be ferromagnetic, while J_4 is antiferromagnetic but very small. Assigning the spins on the metal centers based on the calculated sign of the J values immediately reveals that for **2** the spin ground state is $S = 0$, which arises directly from the noncompeting antiferromagnetic/ferromagnetic interactions: Mn1, Mn4, and Mn6 will be "spin-up", while Mn2, Mn3, and Mn5 will be "spin-down". Although complexes **3** and **4** are different, the structural parameters that control the magnitudes and signs of the J values are very similar and only the strengths of the calculated J values differ between **3** and **4**: J_1 and J_2 are antiferromagnetic, while the remaining interactions are ferromagnetic. Assigning spin-up and spin-down based on the calculated signs of the J values results in an $S = 4$ ground state, with Mn2, Mn4, Mn5, and Mn6 being "spin-up" and Mn1 and Mn3 being "spin-down".

The magnitudes and signs of the DFT-calculated exchange interactions can be rationalized with the structural parameters summarized in Table 8. The interaction between high-spin Mn^{II} ions and high-spin Mn^{III} ions becomes less antiferromagnetic at larger Mn–O–Mn angles.[11b] If there are different bridging units (μ-OR vs μ-O$_2$CR) that mediate the exchange between metal centers, then orbital countercomplementarity effects must also be considered. This changes the energies of the magnetic orbitals, thus greatly influencing the magnetic exchange, and is particularly important when the exchange interactions are small. For example, in the case of J_1, although the angles in **3** and **4** are larger than that in **2**, the strengths of the J values are similar, and this is attributed to the countercomplementary effect of the dissimilar bridging units found in **3** and **4**. The interactions that are responsible for the "switch" in ground state between these two sets of compounds are J_4 and J_5: both interactions are antiferromagnetic in **2** but ferromagnetic in **3** and **4**. Although the Mn–O–Mn angles of all three complexes are close, the additional carboxylate bridges present in **3** and **4** change the nature of the interaction. J_5 describes the interaction between the two central high-spin Mn^{III} ions. Here, larger Mn–O–Mn angles favor an antiferromagnetic interaction (**2**) and smaller Mn–O–Mn angles a ferromagnetic interaction (**3** and **4**). Thus, a subtle change in the angle alters the sign of

Table 8. Structural Parameters and DFT-Calculated *J* Values for **2**−**4**[a]

	complex **2**			complex **3**			complex **4**		
	bridging ligand	d(Mn−Mn) (Å)	J_{DFT} (cm^{-1})	bridging ligand	d(Mn−Mn) (Å)	J_{DFT} (cm^{-1})	bridging ligand	d(Mn−Mn) (Å)	J_{DFT} (cm^{-1})
J_1	μ-OR (2.115; 97.1) μ-OR (2.005; 104.6)	3.177	−7.1	μ-OR (2.162; 116.6) μ-O$_2$CR (2.131; 126.0)	3.685	−7.6	μ-OR (2.100; 118.9) μ-O$_2$CR (2.136; 129.3)	3.621	−5.2
J_2	μ-OR (2.201; 95.8) μ-OR (2.237; 93.8) μ-O$_2$CR (2.117; 130.3)	3.267	−7.8	μ-OR (2.366; 96.7) μ-OR (2.111; 134.5) μ-O$_2$CR (2.108; 135.1)	3.534	−5.0	μ-OR (2.155; 102.9) μ-OR (2.388; 89.6) μ-O$_2$CR (2.129; 131.3)	3.369	−2.2
J_3	μ-OR (2.270; 96.1) μ-OR (2.090; 107.7)	3.337	+2.6	μ-OR (2.073; 104.8) μ-OR (2.149; 99.9)	3.289	+6.8	μ-OR (2.222; 97.2) μ-OR (2.068; 108.3)	3.354	+0.5
J_4	μ-OR (2.098; 99.4) μ-OR (2.034; 103.6)	3.205	−0.9	μ-OR (2.246; 89.5) μ-OR (2.021; 102.7) μ-O$_2$CR (2.090; 257.8)	3.163	+0.2	μ-OR (2.245; 90.3) μ-OR (2.029; 103.2) μ-O$_2$CR (2.069; 129.4)	3.185	+2.1
J_5	μ-OR (2.106; 100.7) μ-OR (2.106; 100.7)	3.250	−6.8	μ-OR (2.117; 98.8) μ-OR (2.117; 98.8)	3.222	+0.7	μ-OR (2.125; 97.7) μ-OR (2.125; 97.7)	3.208	+4.9

[a] All Mn−O distances (Å) are average distances for that particular bridge. The angles (deg) given for the carboxylate ligands are average angles found for the Mn−O−C units.
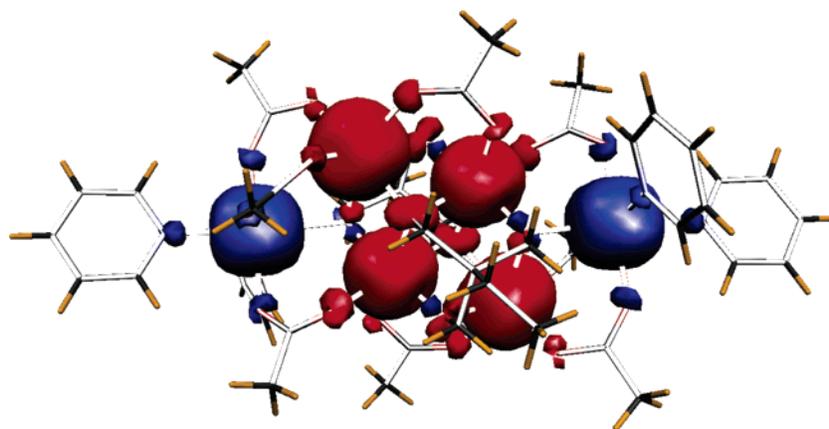
Figure 12. Ground-state spin-density distribution in complex **3**.

J_5 seen in complex **2** to that seen in **3** and **4**, leading to a diamagnetic ground state for **2** and $S = 4$ ground states for **3** and **4**.

The calculated spin-density plot of the ground-state spin structure for complex **3** is shown in Figure 12. The modulus of the spin density on the Mn^{II} and Mn^{III} ions is very close to the free ion values (4.80 and 3.89), and thus very little spin density is distributed to the bridging ligands. The mechanism of the spin-density distribution for the Mn^{II} ions is an interplay between spin delocalization and spin polarization, with the predominant effect being spin delocalization, and thus the ligand atoms coordinated to the metal atoms have the same spin as the metal. For the Mn^{III} ions, both spin delocalization and spin polarization operate, with spin delocalization predominating along the JT elongated axes. Such a spin distribution has been previously observed in a trinuclear Mn^{III} complex.[34]

Conclusions

The use of tripodal alcohols has led to the synthesis of a small family of hexanuclear, mixed-valent, rodlike Mn complexes whose structures are all based on edge-sharing triangles. Despite the structural similarities, their magnetic behavior ranges from diamagnetic ground states to single-molecule magnetism, and this has allowed us to examine the effect that subtle changes in geometry have on the nature of the individual pairwise exchange interactions that govern the resultant ground states. The interactions that are responsible for the *switch* in the ground state from $S = 0$ to 4 between the two sets of compounds differ only in terms of small changes in the bridging angles and in the presence of an additional carboxylate bridge that introduces a counter-complementary effect. Both affect the relative magnitude of the various exchange interactions, ultimately leading to a diamagnetic ground state for **2** and $S = 4$ ground states for **3** and **4**.

Supporting Information Available: Crystallographic data in CIF format. This material is available free of charge via the Internet at http://pubs.acs.org.

IC060676G

(34) Jones, L. F.; Rajaraman, G.; Brockman, J.; Murugesu, M.; Raftery, J.; Teat S. J.; Wernsdorfer, W.; Christou, G.; Brechin, E. K.; Collison, D. *Chem.—Eur. J.* **2004**, *10*, 5180.